Environmental Engineering and Management Journal

July 2019, Vol.19, No. 7, 1079-1095
http://www.eemj.icpm.tuiasi.ro/; http://www.eemj.eu

"Gheorghe Asachi" Technical University of Iasi, Romania

FAST REMOVAL OF MALACHITE GREEN FROM AQUEOUS SOLUTIONS USING HIGHLY HYDROPHOBIC WATER–DISPERSIBLE MAGNETIC NANOCOMPOSITE

Mohsen Nekoeinia[1*], Akram Khodadeh-Tehrani[1], Omran Moradlou[2], Abolfazl Semnani[3], Majid Kolahdoozan[4], Hojjat Kazemi[5], Maryam Kabiri Dehkordi[1]

[1]Department of Chemistry, Payame Noor University, P.O. Box 19395-4697, Tehran, Iran
[2]Department of Chemistry, Faculty of Physics and Chemistry, Alzahra University, P.O. Box: 1993893973, Tehran, Iran
[3]Department of Chemistry, Faculty of Sciences, Shahrekord University, Shahrekord, Iran
[4]Department of Chemistry, Shahreza Branch, Islamic Azad University, Shahreza, Iran
[5]Department of Instrumental Analysis, Research Institute of Petroleum, 14665137 Tehran, Iran

Abstract

Release of dyes without performing adequate treatment into the water can lead to environmental risk and serious health problems. The development of effective and economic adsorbent materials for the removal of dyes from industrial wastewaters has gained great consideration in recent years. In the present study, a novel bio-based nanocomposite has been developed for ultrasound-assisted adsorption of malachite green (MG) from aqueous solutions. The synthesized adsorbent consisting of both hydrophobic surface and hydrophilic polar functional groups was prepared by covalent binding of epoxidized sunflower oil (ESFO) on the surface of silica-coated magnetite nanoparticles. The synthesized sorbent was characterized by FE-SEM, EDS, FT-IR, XRD, VSM and thermal analysis. The effects of experimental parameters including pH, amount of sorbent, temperature and uptake time were investigated for MG adsorption on Fe_3O_4@SiO_2-ESFO sorbent using Box-Behnken design. At the optimized conditions, the adsorption capacity of the magnetic nanocomposite for MG was found to be 4.97 mg g^{-1} according to the removal yield of 90.0%, while 88% of the adsorption occurred at the first 1 min, and the adsorption equilibrium was achieved in few minutes. The results showed that the proposed Fe_3O_4@SiO_2-ESFO sorbent exhibits a strong adsorption affinity to MG, and the adsorption isotherms are well described by Freundlich model. A thermodynamic study of the adsorption indicated that MG adsorption on sorbent was an endothermic and spontaneous phenomena.

Keywords: epoxidation, magnetic nanosorbent, Malachite green, sunflower oil, wastewater treatment

Received: August, 2019; Revised final: December, 2019; Accepted: February, 2020; Published in final edited form: July, 2020

1. Introduction

Paint and painting materials are used extensively in various industries, such as textile, paper and plastic industries as well as foods and cosmetics (Aysu, 2015). So, there is a significant amount of dye effluents in such factories which contaminate the environment every day (Hayat et al., 2015). Due to the increasingly rigorous restrictions on the organic content of industrial effluents, sewage should be purified from such materials before being discharged to the environment (Collivignarelli et al., 2019). Several methods have been used for removing dyes from wastewater, including flocculation (Verma et al., 2012), chemical oxidation and reduction (Hemmati et al., 2018; Nidheesh et al., 2013; Veisi et al., 2019), photocatalytic oxidation (Delsouz Khaki et al., 2017; Zangeneh et al., 2015), as well as biological processes (Sarayu and Sandhya, 2012) and membrane operations (Jirankova et al., 2010).

*Author to whom all correspondence should be addressed: e-mail: m_nekoeinia@pnu.ac.ir; Phone: +98-038-32223328

Although these methods are widely used in pre-treatment of industrial effluents, they suffer from several drawbacks. The main drawbacks of coagulation/flocculation method are the formation of large amounts of sludge-like waste and low effective removal efficiencies of some soluble dyes (Collivignarelli et al., 2019; Verma et al., 2012). Fouling of membrane and high cost of the operation are major problems of the membrane process (Mohammad et al., 2018). Meanwhile, remediation of the industrial effluents containing colorant pollutants by chemical or biological methods is difficult, since most dyes are resistant to oxidizing agents, light and aerobic digestion (Collivignarelli et al., 2019). In recent years, the development of adsorption method has been considered as a promising alternative for treating dyes (Bharathi and Ramesh, 2013; Yagub et al., 2014). This method has several advantages such as low cost, high efficiency, simplicity of operation and possibility of sorbate and adsorbent recovery (Sahan and Ozturk, 2014).

Various natural and synthetic materials such as biomass (Bharathi and Ramesh, 2013; Xiong and Hu, 2019), zeolites (Karadag et al., 2007), activated carbon (Foo and Hameed, 2010; Grigoraș et al., 2020), modified clay (Valipour et al., 2020) and resin (Kaner et al., 2010) have been applied to remove dyes from the effluents. Recently, considerable attention has been devoted for studying dye removal from solution samples by using nano-sized materials (Cai et al., 2017; Ruan et al., 2019). Compared to micro-scale adsorptive agents, nano-sized materials have higher surface area relative to their volume, shorter diffusion path, high adsorption capability and fast extraction dynamics (Giakisikli and Anthemidis, 2013).

Among all nanomaterials, magnetic nanoparticles have attracted increasing interest due to the unique superparamagnetic properties, which can be easily manipulated by influence of an external magnetic field (Giakisikli and Anthemidis, 2013). In order to maintain their specific magnetic properties, and to prevent them from the possible oxidation or agglomeration processes, magnetic nanoparticles are usually coated with organic or inorganic molecules (Faraji et al., 2010). However, the main drawbacks of such coatings are poor wettability and consequently, low dispersion of the resulted sorbent in aqueous solutions because of the hydrophobic groups included in the coated compounds (Tang et al., 2014). So, the removal efficiency of the target molecules from aqueous solutions would be diminished. To address the drawbacks, an efficient approach is to engineer the coatings with both hydrophobic surface and hydrophilic polar functional groups to get good aqueous compatibility (Bai et al., 2010, Tang et al., 2014). For instance, Tang et al. (2014) have coated the hydrophilic methylcellulose on the surface of phenyl-functionalized magnetic nanoparticles and used them as solid phase extraction sorbent to extract sildenafil and desmethylsildenafil from biological samples. The functionalized magnetic nanoparticles have had the excellent dispersibility in aqueous solutions. Luo et al. (2015) have modified the surface of magnetic nanoparticles by both diol and octadecyl (C_{18}) groups. C_{18} groups provide high extraction capability for the non-steroidal anti-inflammatory drugs and the diol groups provide good wettability in the aqueous solutions. Recently, our group has proposed a magnetic wettable hydrophobic nanocomposite for the separation and preconcentration of rhodamine B in aqueous solutions (Nekoeinia et al., 2016). The presence of soybean oil as a hydrophobic surface on the magnetic nanoparticles adsorbs rhodamine B effectively, and the functional groups containing oxygen atoms on the sorbent help to increase the water dispersibility.

Four most important vegetable oilseed crops in the world are palm, soy, rapeseed and sunflower. About 90% of sunflower oil (SFO) unlike other vegetable oils, is used for human consumption and the remaining 10 percent is utilized for industrial application (Jocic et al., 2015). Sunflower oil has a relatively complex composition and typically consists of 5.6-7.6% palmitic, 2.7-6.5% stearic, 14.0-39.4% oleic, and 48.3-74.0% linoleic fatty acids (O'Brien, 2004). Due to the relatively low functionalities of double bonds in SFO and other vegetable oils, it requires modification prior to industrial applications. The double bonds in the chain of SFO can be improved by epoxidation reaction (Bouchareb and Benaniba, 2008). In epoxidation reaction, double bond is replaced by a three-membered epoxide ring, which can easily react with nucleophilic groups (Salimon et al., 2014). The polyols in the middle of the oil chain are formed by ring-opening reaction of epoxide ring in epoxidized sunflower oil (ESFO) with hydroxyl groups of other compounds (Chen et al., 2015).

In this study, magnetic nanoparticles based on epoxidized sunflower oil (Fe_3O_4@SiO_2-ESFO) consisting of a hydrophobic surface and hydroxyl groups as polar functional moieties were synthesized and utilized as a water-dispersible hydrophobic sorbent for fast removal of malachite green (MG). Field-emission scanning electron microscopy (FE-SEM), energy dispersive X-ray spectroscopy (EDS), Fourier transform infrared spectroscopy (FT-IR), X-ray diffraction (XRD), vibrating sample magnetometry (VSM) and thermal analysis (TA) were employed for the characterization of Fe_3O_4@SiO_2-ESFO. Box-Behnken design was used to investigate the roles of four parameters affecting MG removal by Fe_3O_4@SiO_2-ESFO sorbent including temperature, sonication time, pH and sorbent amount. The kinetics, thermodynamic as well as isotherm studies for the adsorption of MG on Fe_3O_4-SiO_2-ESFO were also studied.

2. Material and methods

2.1. Chemicals and apparatus

Iron chloride hexahydrate, iron chloride tetrahydrate, sodium hydroxide, hydrochloric acid, hydrogen peroxide, ethanol, orthophosphoric acid,

tetraethyl orthosilicate (TEOS), malachite green (MG) and triethylamine (TEA) were purchased from Merck. Commercial sunflower oil was provided by Nahangol Co. (Borujen, Iran). A stock solution of MG (250 mgL^{-1}) was prepared by dissolving 0.025 g of MG in a 100 ml doubly distilled water. Phosphate buffer solution containing 0.1 mol L^{-1} total concentration of phosphoric acid was prepared by dissolving appropriate amount of concentrated H_3PO_4 in doubly distilled water and adjusting the pH value to 6.15 by adding appropriate amounts of 0.1 M NaOH solution. The UV-Vis absorption spectra were obtained with double beam UV-Visible spectrophotometer (PG Instrument, T80+). A pH-meter (Milwaukee, MI-180) equipped with a combined glass electrode was applied for measuring pH solutions. The dispersion of the prepared nanoparticles in solution was performed with an ultrasonic water bath (Elma, S30H). Analysis of oil fatty acid composition of SFO was carried out by Agilent 6890 gas chromatograph coupled with flame ionization detector. The FTIR spectra were recorded using Bruker-VERTEX 70 spectrophotometer. The morphology, size and chemical composition of the as-prepared samples were studied by MIRA3 XMU electron microscope equipped with an in-situ energy dispersive X-ray spectrometer (EDS). The XRD patterns of the as-prepared samples were recorded using an X-ray diffractometer (Bruker D8) operated at 40 kV and 100 mA. The magnetic studies were carried out using vibrating sample magnetometer (Meghnatis Daghigh Kavir Co, Iran). Thermal analysis studies under N_2 atmosphere were performed using a simultaneous thermal analyzer (STA, BAHR 503).

2.2. Synthesis of Fe_3O_4@SiO_2-ESFO

The epoxidized sunflower oil (ESFO) was prepared by in situ peracid generation method (Lee et al., 2008). Refined SFO (40.0 g), H_2O_2 (15.0 g), glacial acetic acid (6.0 g) and concentrated H_2SO_4 (0.25 g) were refluxed for 5 h at 50 ^{0}C. Then, the mixture was transferred into a separatory funnel and the organic phase containing ESFO was separated. The traces of acid present in the reaction mixture were removed by washing the organic phase with 50.0 mL of doubly distilled water for four times.

Fe_3O_4 and Fe_3O_4@SiO_2 nanoparticles were prepared according to our previously reported procedure (Nekoeinia et al., 2016). For the synthesis of the Fe_3O_4@SiO_2-ESFO, 4.3 g of Fe_3O_4@SiO_2, 4.0 mL of ESFO, 20.0 mL of 1,4-dioxane and 0.1 mL of TEA were added in a 250 mL round-bottom flask and stirred for 24 h at room temperature. The obtained magnetic nanoparticles were separated by external magnet, washed two times with doubly distilled water and dried at 80 °C for 16 h. The chemical route for the preparation of Fe_3O_4@SiO_2-ESFO is shown schematically in Fig. 1.

2.3. Dye removal procedure

Adsorption process of MG on Fe_3O_4@SiO_2-ESFO was investigated in a batch system. In all experiments, 100.0 mL of an aqueous solutions containing 15 mg L^{-1} of MG were used. The pH of solution was adjusted to a desired value (3.0, 5.0 and 7.0) with 0.1 mol L^{-1} phosphoric acid and NaOH solution (0.1 mol L^{-1}). After that, proper amount of sorbent (0.1-0.3 g) was added and the temperature of the solution was maintained at 30 to 60°C. In order to effective removal of MG from aqueous solution, the flask was immersed in an ultrasonic bath for 2 to 6 min (Elma S30H, Italy) operating at the frequency of 37 kHz and effective power output of 80 W. The sorbent was isolated by an external magnet and the supernatant was decanted. The percentage of removal efficiency (R(%)) of MG on Fe_3O_4@SiO_2-ESFO was obtained by (Eq. 1):

$$R(\%) = \frac{A_0 - A}{A_0} \times 100 \qquad (1)$$

where, A_0 and A are the absorbance of MG solution at 617 nm before and after sonication, respectively.

2.4. Optimization

Box-Behnken Design (BBD) at three levels for four factors was applied to obtain the highest sorption percentage of MG on Fe_3O_4@SiO_2-ESFO sorbent. Sorbent amount (g), pH, sonication time (min), and temperature (°C) were considered as independent variables and the sorption percentage of MG was delimited as dependent variable. The experimental dominions of the four independent variables were found by primary experiments.

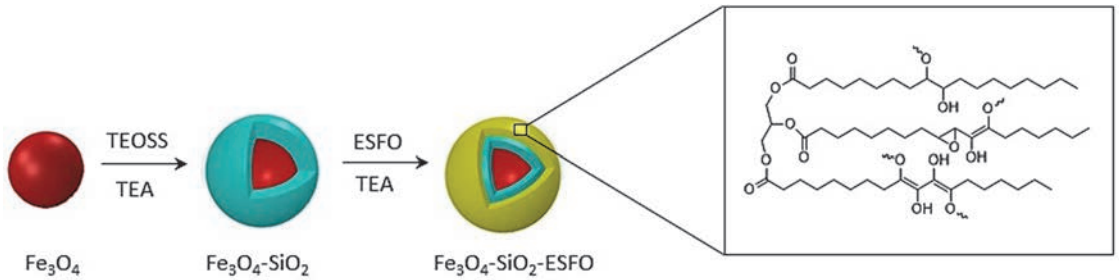

Fig. 1. Schematic illustration for the synthesis of Fe_3O_4@SiO_2-ESFO nanoparticles

The symbols and levels of the used factors in BBD are given in Table 1. According to BBD, the mathematical equation which describes the relation between estimated response (R), and coded independent variables (x_i and x_j) is as follows (Bingöl et al., 2012):

$$R = \beta_0 + \sum_{i=1}^{n} \beta_i x_i + \sum_{i=1}^{n} \beta_{ii} x_i^2 + \sum_{1 \le i \le j}^{n} \beta_{ij} x_i x_j + \varepsilon \quad (2)$$

where, β_0, β_i, β_{ii} and β_{ij} are constant, linear, quadratic and interactive coefficients, respectively, and ε is the random error. The coded values of the variables can be calculated using the (Eq. 3) (Bingöl et al., 2012):

$$x = \frac{X - \left| \frac{X_{max} + X_{min}}{2} \right|}{\left| \frac{X_{max} - X_{min}}{2} \right|} \quad (3)$$

where, x and X are the coded and real values of the variables, respectively. Also, X_{max} and X_{min} are the maximum and minimum values of each real variables, respectively.

2.5. Equilibrium studies

Adsorption isotherms were obtained by adding 0.27 g of the Fe_3O_4@SiO_2-ESFO to 100 mL of MG solution with different initial concentrations (2.5 to 15 mg L^{-1}) at pH 6.15. The flasks were sonicated in ultrasonic bath at the desired temperature (30^0C) for 15.0 min until equilibrium was reached. The sorption capacity q_e (mg g^{-1}) was calculated by using the (Eq. 4):

$$q_e = \frac{(C_0 - C_e)V}{m} \quad (4)$$

where, C_0 and C_e represent the initial and equilibrium concentrations of MG in the solution (mg L^{-1}), respectively; V is the volume of solution (L) and m is the sorbent mass (g).

2.6. Kinetic studies

The kinetic studies were investigated by adding 0.27 g of the Fe_3O_4@SiO_2-ESFO to 100 mL of MG solution with initial concentration of 15 mg L^{-1}. All the kinetic experiments were performed at 30^0C. The MG solution containing adsorbent was sonicated in ultrasonic bath. The aqueous samples were taken at the preset time intervals and the concentration of MG in each sample was measured.

3. Results and discussion

3.1. Characterization studies

At first, sunflower oil (SFO) was converted to epoxidized sunflower oil (ESFO) by using in-situ peracid approach. In the presence of H_2SO_4, hydrogen peroxide reacts with CH_3COOH and peracid is formed (Dinda et al., 2008). In the epoxidation reaction, double bonds in SFO are replaced by a three-membered epoxide ring and ESFO is obtained. As the FT-IR spectra of SFO and ESFO show (Fig. 2a), strong bands at 1160 and 1744 cm^{-1} are assigned to the vibrational stretching modes of C-O and C=O ester bonds, respectively (Purbaya et al., 2015). The strong band at 1463 cm^{-1} is related to the vibrational mode of C-H bending. Also, strong peak observed at 722 cm^{-1} is due to rocking and bending vibrational modes of CH_2 in SFO and ESFO (Purbaya et al., 2015). The band at 3008 cm^{-1} in SFO corresponds to C-H stretching vibration of the cis-double bond. The 2853 and 2923 cm^{-1} bands are related to vibration of C-H bond (stretching) in raw and epoxidized oil chains (Purbaya et al., 2015). The band at 3008 cm^{-1} in SFO corresponds to C-H vibration (stretching) of the cis-double bond (Vlachos et al., 2006). In comparison with the spectrum of SFO, the appearance of two weak bands at 844 and 871 cm^{-1} and near complete disappearance of the band at 3008 cm^{-1} are observed in FT-IR spectrum ESFO.

These observations indicated the successful formation of ESFO which is consistent with previous reports (Narute and Palanisamy, 2015; Vlček and Petrović, 2006). The efficiency of oil epoxidation reaction was measured by iodine value, which is defined as the grams of iodine (I_2) reacted per 100 g of sample (O'Keefe and Pike, 2010). The iodine values for SFO and ESFO were obtained to be 79.00 and 32.51 g of I_2/100 g of oil, respectively. In the epoxidation process, the unsaturated bonds in SFO are converted to oxirane groups and iodine value tends to lower value due to the lack of carbon-carbon double bonds in ESFO. FT-IR spectra shown in Fig. 2b demonstrate the successful fabrication of Fe_3O_4, Fe_3O_4@SiO_2 and Fe_3O_4@SiO_2-ESFO.

Table 1. The experimental variables and levels of the Box-Behnken Design

Variables	*Symbols*		*Levels*		
	Uncoded	*Coded*	*Low*	*Middle*	*High*
pH	X_1	x_1	3	5	7
Uptake time (min)	X_2	x_2	2	4	6
Temperature (°C)	X_3	x_3	30	45	60
Sorbent mass (g)	X_4	x_4	0.1	0.2	0.3

The bands appeared in FT-IR spectrum at 438, 584, and 635 cm^{-1} assigned to Fe-O bond, correspond to the formation of Fe_3O_4 (Rahimi et al., 2014). Two weak and strong bands at 803 and 1087 cm^{-1} appeared in FT-IR spectrum of Fe_3O_4@SiO_2 which belong to the Si-O-Fe and Si-O-Si vibrations, respectively, confirming the formation of silica shell on magnetite nanoparticles. The bands appeared around 3424 and 1624 cm^{-1} are assigned to O-H vibrations of water

remaining in the two magnetic samples (Rahimi et al., 2014). The bands at 2854, 2925, 1745 and 1462 cm^{-1} that belong to functional groups of ESFO showed that Fe_3O_4@SiO_2 has been coated by epoxidized oil. By comparing these spectra, the bands assigned to O-H vibrations of remaining water (3424 and 1624 cm^{-1}) were disappeared and the weak bands were observed around 3400 cm^{-1} which correspond to the vibrations of hydroxyl group, due to the ring-opening reaction of epoxide rings or the presence of trace water (Barcena et al., 2017).

This result indicated that surface of Fe_3O_4@SiO_2 was successfully modified by ESFO. Fig. 3 shows the XRD patterns of three synthesized magnetic samples. The distinct peaks located at 2θ values of 30.2, 35.7, 43.4, 57.2 and 63.0° are assigned to (220), (311), (400), (511) and (440) crystal planes of pristine magnetite, respectively (Panahi et al., 2018). Also, the results showed that upon modification of the magnetite core surface by SiO_2 and ESFO, no significant peak position shifts of Fe_3O_4 were observed and only peak intensities were decreased. The similar diffraction patterns of Fe_3O_4@SiO_2-ESFO and Fe_3O_4@SiO_2 with Fe_3O_4 indicate that after modification reactions of magnetite cores, crystalline phase of Fe_3O_4 is not changed. The magnetization curves of three synthesized samples are shown in Fig. 4. The magnetization curves of all three prepared samples have not shown any hysteresis loop, which indicated that Fe_3O_4, Fe_3O_4@SiO_2 and Fe_3O_4@SiO_2-ESFO were superparamagnetic behavior. As it is clear from the magnetization curves, the saturation magnetizations of pristine Fe_3O_4, Fe_3O_4@SiO_2 and Fe_3O_4@SiO_2-ESFO were 39.7, 31.8 and 23.3 emu/g, respectively. Decrease in the saturation magnetization can be attributed to the modification of magnetite core surface by SiO_2 and ESFO. The results revealed that the epoxidized sunflower oil modified magnetic nanoparticles still exhibit a good magnetic response, indicating that Fe_3O_4@SiO_2-ESFO could be used as a potential magnetic sorbent. Thermal analysis results of Fe_3O_4@SiO_2-ESFO are shown in the Fig. 5. As it is clear from the thermal gravimetric analysis (TGA) curve, the first percentage mass loss is 3.5% and is occurred gradually at 30-330°C which corresponds to exclusion of free ESFO and residual solvents of synthetic procedure from the surface of as-prepared sorbent.

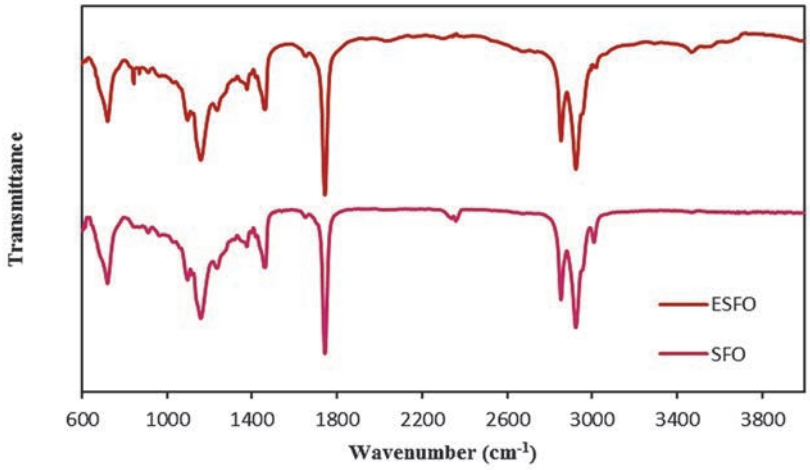

(a)

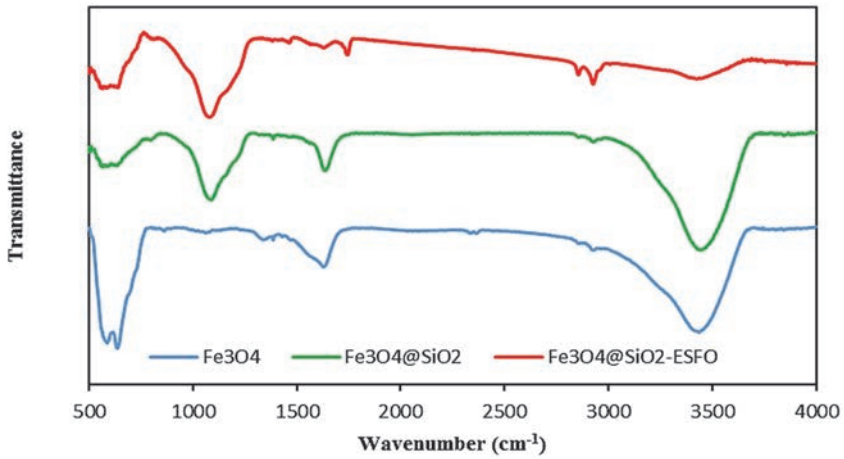

(b)

Fig. 2. FTIR spectra of SFO and ESFO (a); Fe_3O_4, Fe_3O_4@SiO_2 and Fe_3O_4@SiO_2- ESFO (b)

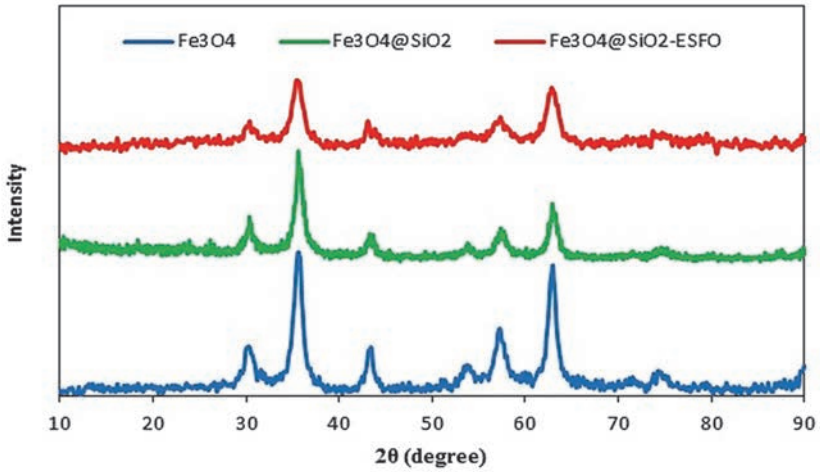

Fig. 3. XRD patterns of Fe_3O_4, Fe_3O_4@SiO_2 and Fe_3O_4@SiO_2-ESFO

The broad endothermic peak at 214°C in the differential thermal analysis (DTA) plot is attributed to the first stage of mass loss in the TG curve. The second mass loss is about 8.0% and happens at 330-450°C. This mass loss corresponds to an endothermic peak at 411°C in DTA plot and it can be attributed to the removal of ESFO which bonds chemically to the surface of Fe_3O_4@SiO_2. The high desorption temperature reflects a strong interaction between ESFO and hydroxyl groups present on the surface of Fe_3O_4@SiO_2. The third endothermic peak at around 740 °C in DTA curve indicates the phase transition from Fe_3O_4 to FeO (Zhao et al., 2006). The surface morphology of Fe_3O_4, Fe_3O_4@SiO_2 and Fe_3O_4@SiO_2-ESFO were studied by FE-SEM. The FE-SEM images of the synthesized samples are shown in Fig. 6. As it is clear, the morphology of pristine Fe_3O_4 is spherical and uniform with severe aggregation due to their magnetic nature. The particle size of the Fe_3O_4 is found to be about 20 nm. Figs 6b and 6c show the FE-SEM images of as-prepared Fe_3O_4@SiO_2 and Fe_3O_4@SiO_2-ESFO. These images shows that the morphology of the modified Fe_3O_4 was not changed upon modification of the magnetite core surface by SiO_2 and ESFO. The SEM-EDS spectrum of the Fe_3O_4@SiO_2-ESFO (Fig. 6d) shows the presence of Fe, Si, O and C elements in the prepared nanosorbent.

3.2. Optimization of conditions for MG removal

Preliminary experiments of the sorption of MG by 0.15 g of unmodified and modified Fe_3O_4@SiO_2 at pH 5.0 indicated that the sorption efficiency of MG was 21.01±3.61% and 58.32±2.20%, respectively. Based on the preliminary results, it was also found that the bonded ESFO on the surface of Fe_3O_4@SiO_2 exhibits a noticeable effect on the adsorption of MG.

To achieve the highest sorption percentage, the conditions of MG sorption on nanosorbent should be optimized. The optimization conditions of the MG sorption onto Fe_3O_4@SiO_2-ESFO were evaluated using BBD. The experimental variables, their levels and the corresponding results of experiments are given in Table 2.

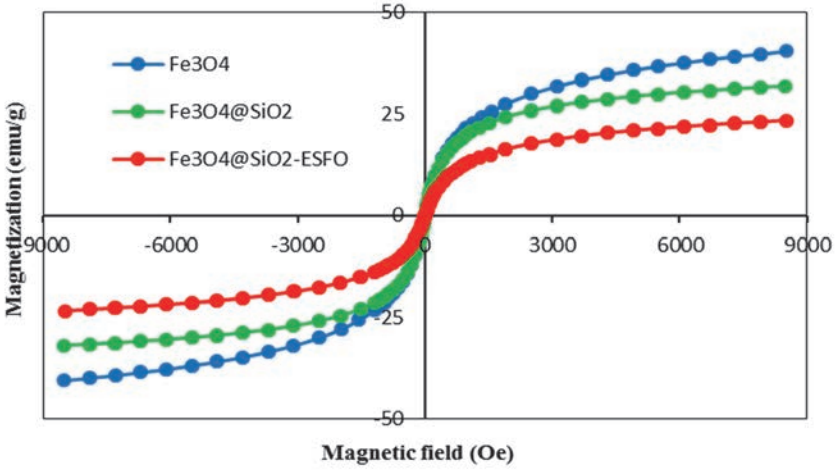

Fig. 4. Magnetization curves of Fe_3O_4, Fe_3O_4@SiO_2 and Fe_3O_4@SiO_2-ESFO

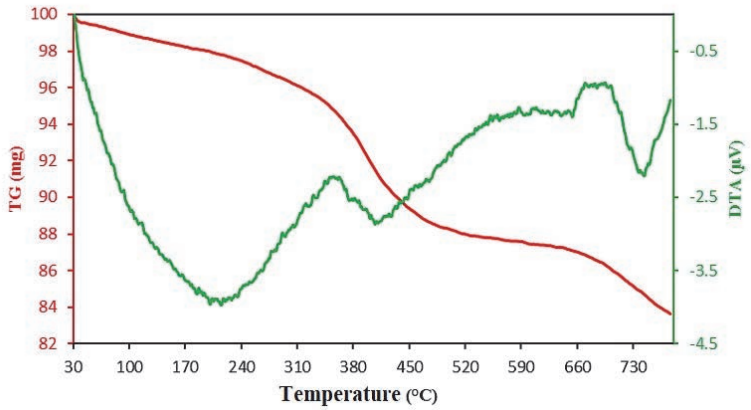

Fig. 5. TG and DTA curves of Fe_3O_4@SiO_2-ESFO

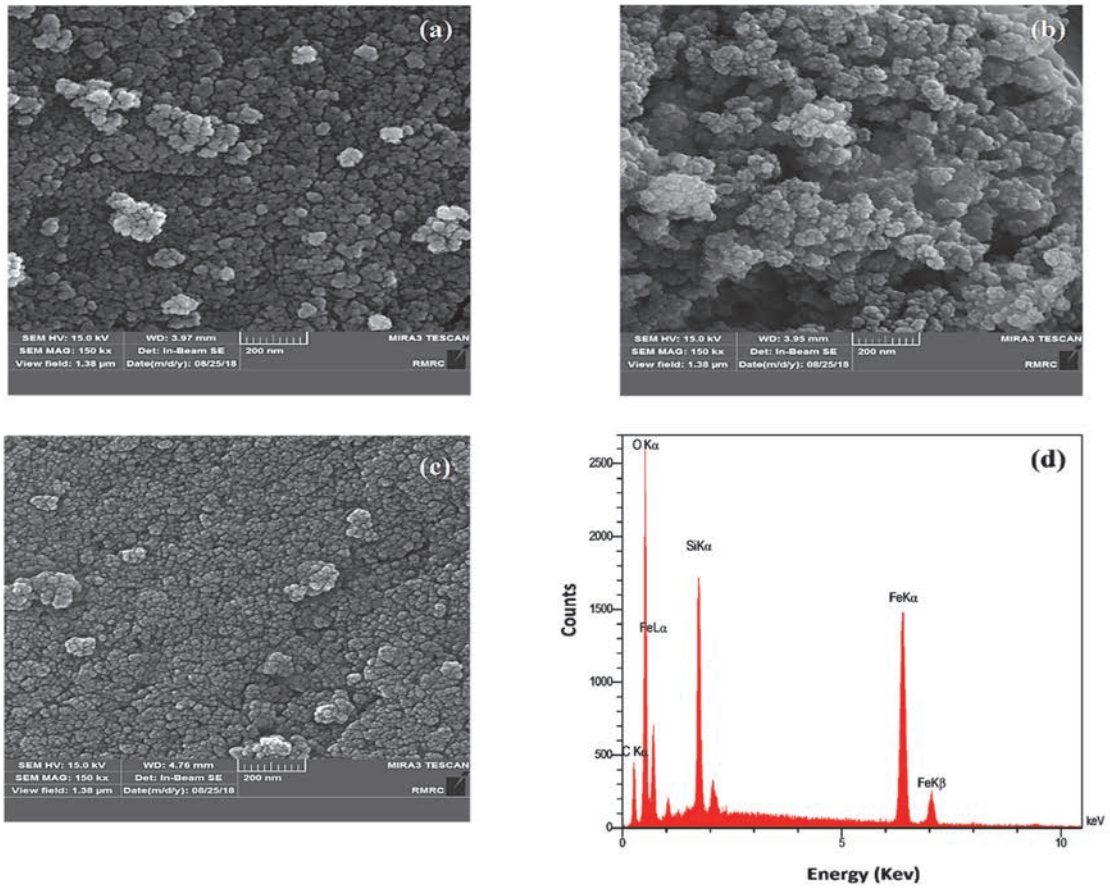

Fig. 6. FE-SEM images of Fe_3O_4 (a), Fe_3O_4@SiO_2 (b) and Fe_3O_4@SiO_2-ESFO (c); EDS spectrum of Fe_3O_4@SiO_2-ESFO (d)

The analysis of variance was applied to evaluate the significance of the model and the parameters statistically. According to ANOVA table (Table 3), the F-value of the model was 56.20. The calculated F-value is higher than the tabulated F value at 5% ($F_{14,12}$ =2.63), suggesting that the empirical model is statistically significant. The coefficient of determination (R^2), adjusted coefficient of determination (R_{adj}^2) and lack of fit were used for the evaluation of the goodness of fit of the empirical model. R^2 and R_{adj}^2 values of obtained model were 0.9850 and 0.9675, respectively. According to R^2 value, only 1.5% of the total variations are not described by empirical model. In addition, R_{adj}^2 value is very close to 1, indicating that the empirical model is appropriate for describing the experimental results. The probability value of lack of fit is greater than 0.05, which suggests that the lack of fit is not statistically significant relative to pure error. These results demonstrate that the empirical model equation is adequate for predicting the removal efficiency of MG by Fe_3O_4@SiO_2-ESFO sorbent. The level of

significance of each model term on sorption efficiency was checked by P-values. The values lower than 0.05 indicate that the corresponding coefficient terms are statistically significant (Maiti et al., 2011). According to ANOVA Table, X_1, X_2, X_1^2, X_4^2, X_1X_4 are significant model terms for the sorption of MG. The mathematical equation which describes the relation between MG sorption percentage (R) and coded significant variables is expressed by the (Eq. 5):

$$R = 78.33+18.224x_1+2.328x_2–2.707x_3+12.307x_4– -9.00x_1^2–8.91x_4^2–8.76x_1x_4 \quad (5)$$

where, x_1, x_2, x_3 and x_4 are coded values of the pH of experiment, sonication time, temperature and sorbent amount, respectively. Also, visual evaluation of the proposed model was depicted by the parity plot (Fig. 7). As it is clear, a good correlation exists between the observed and predicted values of MG removal efficiency.

Table 2. Design matrix in the Box-Behnken model, observed and predicted values

Runs	Actual level of factors				Coded level of factors				Removal efficiency	
	X_1	X_2	X_3	X_4	x_1	x_2	x_3	x_4	Observed	Predicted
1	7	2	45	0.2	+1	–1	0	0	85.43	84.42
2	5	2	45	0.1	0	–1	0	–1	53.29	55.62
3	7	4	45	0.1	+1	0	0	–1	75.84	75.09
4	3	4	45	0.3	–1	0	0	+1	63.65	63.26
5	5	4	45	0.2	0	0	0	0	80.09	78.33
6	5	4	60	0.1	0	0	+1	–1	53.64	56.77
7	3	4	30	0.2	–1	0	–1	0	51.66	55.46
8	3	2	45	0.2	–1	–1	0	0	47.53	46.25
9	7	4	45	0.3	+1	0	0	+1	80.88	82.19
10	5	4	45	0.2	0	0	0	0	76.51	78.33
11	3	4	45	0.1	–1	0	0	–1	23.58	21.13
12	7	6	45	0.2	+1	+1	0	0	85.54	87.35
13	5	2	60	0.2	0	–1	+1	0	71.9	71.40
14	5	2	45	0.3	0	–1	0	+1	71.9	75.23
15	5	6	45	0.3	0	+1	0	+1	86.63	84.89
16	3	6	45	0.2	–1	+1	0	0	51.08	52.62
17	7	4	60	0.2	+1	0	+1	0	89.71	86.50
18	5	4	60	0.3	0	0	+1	+1	77.02	77.09
19	3	4	60	0.2	–1	0	+1	0	48.42	47.18
20	5	6	30	0.2	0	+1	–1	0	82.11	81.47
21	5	4	45	0.2	0	0	0	0	78.4	78.33
22	5	6	45	0.1	0	+1	0	0	58.01	55.27
23	5	4	30	0.1	0	0	–1	–1	57.42	57.88
24	5	4	30	0.3	0	0	–1	+1	89.39	86.79
25	5	6	60	0.2	0	+1	+1	0	75.21	76.95
26	5	2	30	0.2	0	–1	–1	0	80.59	77.71
27	7	4	30	0.2	+1	0	–1	0	87.21	89.04

Table 3. Analysis of variance (ANOVA) for Box-Behnken design

Source of variation	Df [a]	SS [b]	MS [c]	F value	P value [d]
Model	14	7124.73	508.91	56.2	0.000
X_1	1	3985.44	3985.44	440.15	0.000
X_2	1	65.05	65.05	7.18	0.02
X_3	1	87.91	87.91	9.71	0.009
X_4	1	1817.69	1817.69	200.74	0.000
X_1^2	1	432.2	432.2	47.73	0.000
X_2^2	1	14.8	14.8	1.63	0.225
X_3^2	1	0.25	0.25	0.03	0.871
X_4^2	1	423.6	423.6	46.78	0.000
$X_1 \times X_2$	1	2.96	2.96	0.33	0.578
$X_1 \times X_3$	1	8.24	8.24	0.91	0.359
$X_1 \times X_4$	1	306.78	306.78	33.88	0.000
$X_2 \times X_3$	1	0.8	0.8	0.09	0.771
$X_2 \times X_4$	1	25.05	25.05	2.77	0.122
$X_3 \times X_4$	1	18.45	18.45	2.04	0.179
Lack-of-Fit	10	102.24	10.22	3.19	0.262
Pure Error	2	6.41	3.21		
Total	26	7233.39			

[a] degree of freedom [b] Sum of square [c] Mean square [d] p values <0.05 were considered to be significant

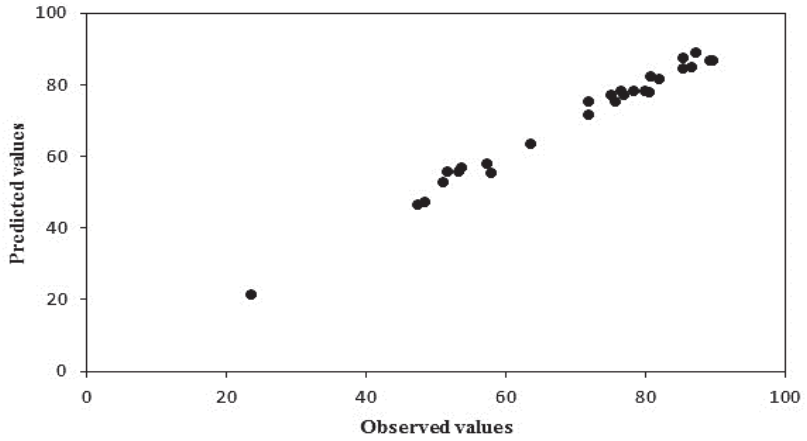

Fig. 7. Parity plot of the observed and predicted values of the MG removal efficiency

Fig. 8 illustrates the three-dimensional response surface plots for the relationships between four factors on the sorption of MG onto Fe_3O_4@SiO_2-ESFO. These plots are established as a function of two experimental factors while the other factors are fixed at their central levels. It can be seen that pH, sonication time and sorbent mass have positive mutual impact on sorption efficiency of MG. In addition, plots showed that the sonication time and temperature have smaller effects on the sorption efficiency of MG compared with pH and sorbent mass. Based on the overall results of the optimization study, pH value of 6.15, sorbent amount of 0.27 g, temperature of 30°C, and sonication time of 5.8 min are obtained as the optimal conditions.

The pH at which the net charge of the sorbent surface is zero, is defined as point of zero charge (pH_{pzc}) (Fiol and Villaescusa, 2009). Mass titration procedure was used for the determination of pH_{pzc} of Fe_3O_4@SiO_2-ESFO (Ẑalac and Kallay, 1992). The pH_{pzc} of Fe_3O_4@SiO_2-ESFO was found to be 7.38. According to the concept of pH_{pzc}, the surface of sorbent should be positive at pH values <7.38 and negative at pH values >7.38. In the solution with the pH value of 6.15 (optimal condition), the MG molecule exists in its cationic form (Savva et al., 2015), which theoretically cannot be adsorbed on Fe_3O_4@SiO_2-ESFO mainly because of the electrostatic repulsion between likely charged MG molecules and adsorbent surface at pH 6.15. So, according to the obtained high removal efficiency of MG on proposed sorbent at pH 6.15, the electrostatic attraction would not be a noticeable interaction between MG and Fe_3O_4@SiO_2-ESFO. These results suggested that the other interactions such as hydrogen bonding and hydrophobic-hydrophobic attraction may be involved. Similar behaviors have also been reported in the adsorption of cationic and anionic dyes (Al-Degs et al., 2008; Kooh et al., 2016).

3.3. Adsorption isotherm

The adsorption isotherm quantitatively describes the equilibrium distribution of single sorbate species between the solution and the solid phase (El-Sayed, 2011). Hence, the isotherm contains the information about the interactions between the sorbent and the sorbate species (Guimarães Gusmão et al., 2012). Distribution of the sorbate species between the solution phase and solid phase can be described by several isotherm models. To find the most appropriate model for the sorbate species onto the sorbent, the obtained experimental data are fitted to various types of adsorption isotherm models including Langmuir, Temkin and Freundlich isotherm models.

The Langmuir isotherm assumes that the adsorption of sorbate species occurs on a homogeneous surface by a limited number of identical sorption sites without interaction between sorbate species. In contrast, Freundlich isotherm is an empirical model and can be applied to describe an adsorption process that takes place on heterogeneous surfaces. According to the Freundlich isotherm model, the binding sites are not equivalent or independent, and so, the amount of sorbate species increases infinitely with increasing concentration (Huang et al., 2016). The Temkin model isotherm explains sorption processes by assuming that the heat of adsorption of the sorbate species decreases linearly with adsorbent layer coverage (El-Sayed, 2011; Fonseca et al., 2009). Linear forms of isotherm models are stated by the Eqs. (6-8).

Langmuir equation:

$$\frac{1}{q_e} = \frac{1}{K_L q_{\max}} \frac{1}{C_e} + \frac{1}{q_{\max}} \tag{6}$$

Freundlich equation:

$$\ln q_e = \ln K_F + \frac{1}{n} \ln C_e \tag{7}$$

Temkin equation:

$$q_e = B \ln A + B \ln C_e \tag{8}$$

where, q_e (mg g^{-1}) is the amount of sorbate species adsorbed at equilibrium time and C_e (mg L^{-1}) is the equilibrium concentration of sorbate species in the solution.

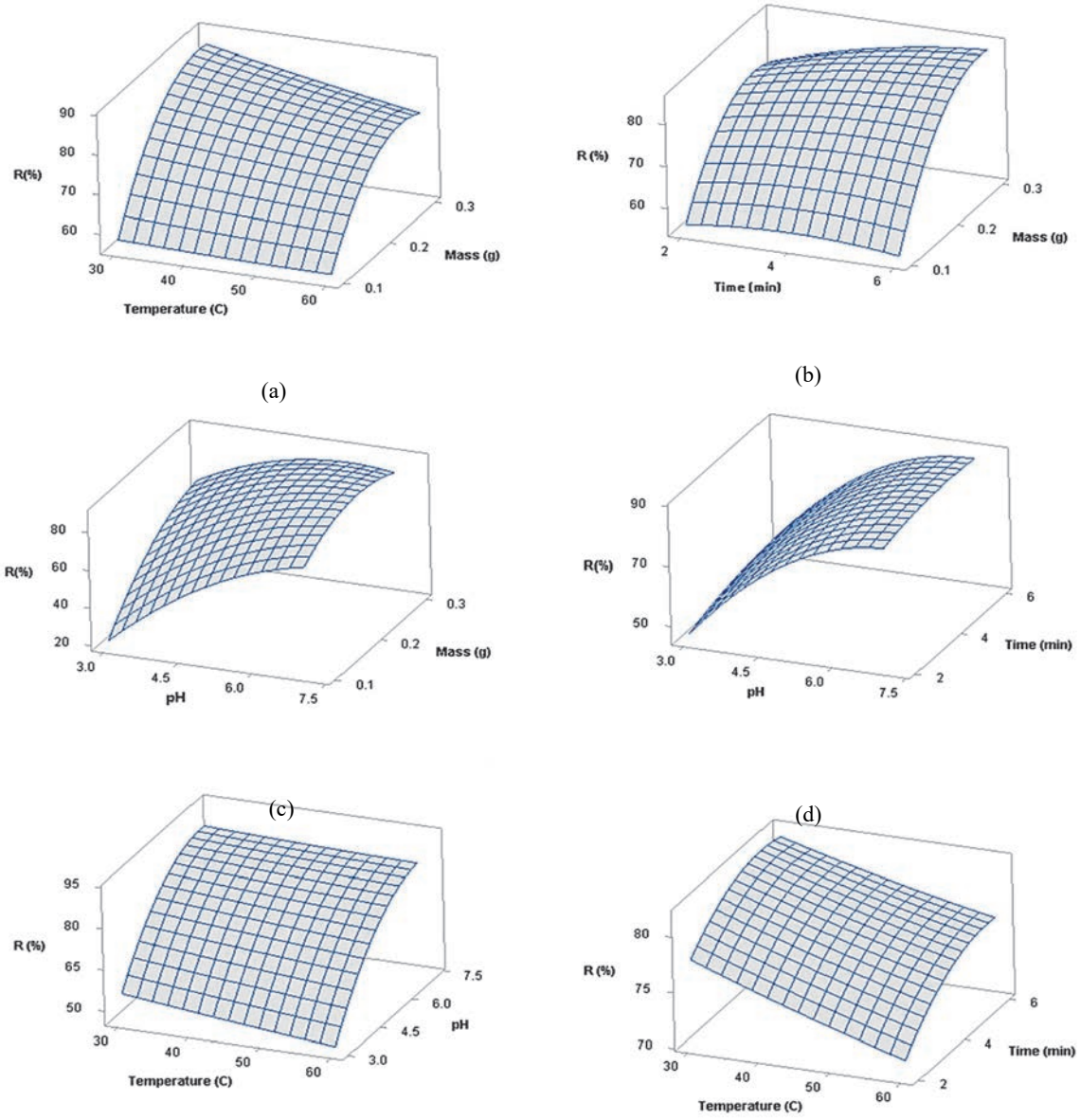

Fig. 8. 3-D response surface of the percentage of removal efficiency R(%) as a function of temperature and sorbent mass (a), uptake time and sorbent mass (b), pH and sorbent mass (c), pH and uptake time (d), temperature and pH (e) and temperature and uptake time (f)

The other parameters are determined by fitting the experimental data. In the Langmuir equation, q_{max} (mg g^{-1}) and K_L (L mg^{-1}) are the maximum quantity of a sorbate species per unit sorbent and Langmuir adsorption constant, respectively. The K_F (L mg^{-1}) and *1/n* are constants in the Freundlich equation, which is roughly related to the sorption capacity and intensity, respectively. The degree of deviation from linearity between solution concentration and adsorption is determined by *n* value (Senthil Kumar et al., 2010). In the Temkin isotherm, it is assumed that heat of adsorption of all sorbate species is decreased linearly with increase in the surface coverage (Senthil Kumar et al., 2010). In the Temkin equation, *A* (L g^{-1}) is the equilibrium binding constant and *B* is expressed as *RT/b*, where *R* is gas constant (8.314 J/mol K) and *T* is the absolute temperature (K). The heat of sorption is described by the Temkin constant *b* (J mol^{-1}).

Isotherm models of Langmuir, Freundlich and Temkin in the adsorption of MG have been shown in Fig. 9. The estimated model parameters which are obtained from the slope and intercept of the plots for these different models are displayed inside the figures. The Langmuir isotherm model shows a good fit (R^2=0.981), but the values of K_L and q_{max} are negative, indicating that the proposed model for explaining the adsorption process is inadequate. The low value of the determination of coefficient (R^2=0.956) suggests that Temkin model is not appropriate for the present study. In comparison with Langmuir and Temkin isotherms, the Freundlich isotherm yieldes the best fit with the highest R^2 value (0.991). According to the linear form of Freundlich isotherm model, the values of K_F and *n*

are 2.138 and 0.619, respectively. The value of *n* is smaller than unity that indicates the sorption of dye on magnetic sorbent can be difficult at higher MG concentrations (Avisar et al., 2010). The decrease in the sorption at higher MG concentrations may be ascribed to the saturation of specific binding sites on sorbent or less tendency of MG molecules to adsorb on remaining sites (Kulshrestha et al., 2004). These results indicate that the sorption of MG is occurred on heterogeneous surface of Fe_3O_4@SiO_2-ESFO with energetically non-uniform distribution binding sites.

3.4. Adsorption kinetics

Adsorption kinetics describe the uptake rate of dissolved sorbate species from the solution. The changes in MG sorption capacity on proposed sorbent as a function of time were depicted in Fig. 10. There are two main steps in the adsorption of MG on Fe_3O_4@SiO_2-ESFO. In the initial step, the rate of MG adsorption on nanosorbent was very fast and about 88% of the adsorption was occurred in the first 1 min. In the second step, the adsorption capacity continued to rise slightly for the next time and finally reached to its equilibrium value. The inset of Fig. 10 shows the photographs that were taken during MG adsorption by proposed nanocomposite before contact and at the contact time of 1 min, indicating the rapid MG removal by the proposed Fe_3O_4@SiO_2-ESFO.

To study the kinetics of MG adsorption on Fe_3O_4@SiO_2-ESFO, the experimental data were fitted to the pseudo-first order and pseudo-second order models. Pseudo-first order (Eq. 9) and pseudo-second order (Eq. 10) models are expressed by the following Equations (Hameed et al., 2007; Ho et al., 1996):

$$\log(q_e - q_t) = \log q_e - \frac{k_1 t}{2.303} \tag{9}$$

$$\frac{t}{q_t} = \frac{1}{k_2 q_2^e} + \frac{1}{q_e} t \tag{10}$$

where, q_e is the sorption capacity of sorbent at equilibrium, q_t is the sorption capacity of sorbent at time *t*. The k_1 and k_2 are the pseudo-first order (min^{-1}) and pseudo-second order ($gmg^{-1}min^{-1}$) rate constants, respectively.

The results for the fitting of the experimental data to pseudo-first order and pseudo-second order models were presented in Table 4. The determination coefficient value of the pseudo-second order kinetic model (R^2=0.999) was higher than that of the pseudo-first order kinetics model (R^2=0.939), which shows that the pseudo-second order model better describes the kinetic data (Fig. 11).

3.5. Adsorption thermodynamics

The feasibility and spontaneity nature of the sorption process at desired temperature is described by thermodynamic studies. Thermodynamic parameters of sorption process including ΔG^o, ΔH^o and ΔS^o are calculated by Equations (11-13) as follows:

$$K_C = \frac{C_A}{C_S} \tag{11}$$

$$\Delta G° = -RT \ln K_C \tag{12}$$

$$\ln K_C = \frac{-\Delta H°}{RT} + \frac{\Delta S°}{R} \tag{13}$$

where, C_A and C_S are the concentration of MG on the sorbent and in the solution (mg L^{-1}), respectively. *T*, *R* and K_C are absolute temperature, gas constant, and equilibrium constant of the sorption process, respectively.

The plot of $ln\ K_C$ versus $1/T$ (Fig. 12) yields a straight line with the R^2 value of 0.984. The change in standard enthalpy (ΔH^o) and change in standard entropy (ΔS^o) were obtained from the slope and intercept, respectively. The negative value of ΔG^o and positive value of ΔH^o in Table 5 imply that the MG adsorption on Fe_3O_4@SiO_2-ESFO is a spontaneous and endothermic phenomenon.

3.6. Adsorption of other dyes and industrial application

Apart from MG, two other commercial cationic dyes (crystal violet and methylene blue) were also examined to verify the adsorption activity of Fe_3O_4@SiO_2-ESFO. The removal efficiencies of crystal violet and methylene blue were 85.1% and 79.3%, respectively, when adsorption experiments were conducted under the optimal experimental conditions of MG adsorption on Fe_3O_4@SiO_2-ESFO. The results demonstrate that the prepared adsorbent can efficiently adsorb a variety of organic dyes from aqueous solutions. Also, to explore the industrial sample applicability of the prepared adsorbent, wastewater samples from textile company (Hejab Textile Co., Shahrekord, Iran) was treated by using Fe_3O_4@SiO_2-ESFO adsorbent. Under the optimized conditions, Fe_3O_4@SiO_2-ESFO removed nearly 70% of dye residues in wastewater sample, indicating that the proposed adsorbent is suitable for removal of dye residues from real textile wastewater samples.

3.7. Comparison with other reported magnetic adsorbent

The comparison of adsorption capacity, uptake time and removal efficiency of some magnetic adsorbents of Fe_3O_4@SiO_2-ESFO and other adsorbents in the literature was presented in Table 6. As can be seen, although the adsorption capacity of Fe_3O_4@SiO_2-ESFO is not high, but the removal efficiency of the proposed adsorbent is comparable with those of other reported adsorbents. In addition, Fe_3O_4@SiO_2-ESFO shows a better uptake time compared to the reported magnetic adsorbents. The results reported in this study showed that the prepared composite is an appropriate adsorbent for the removal of MG.

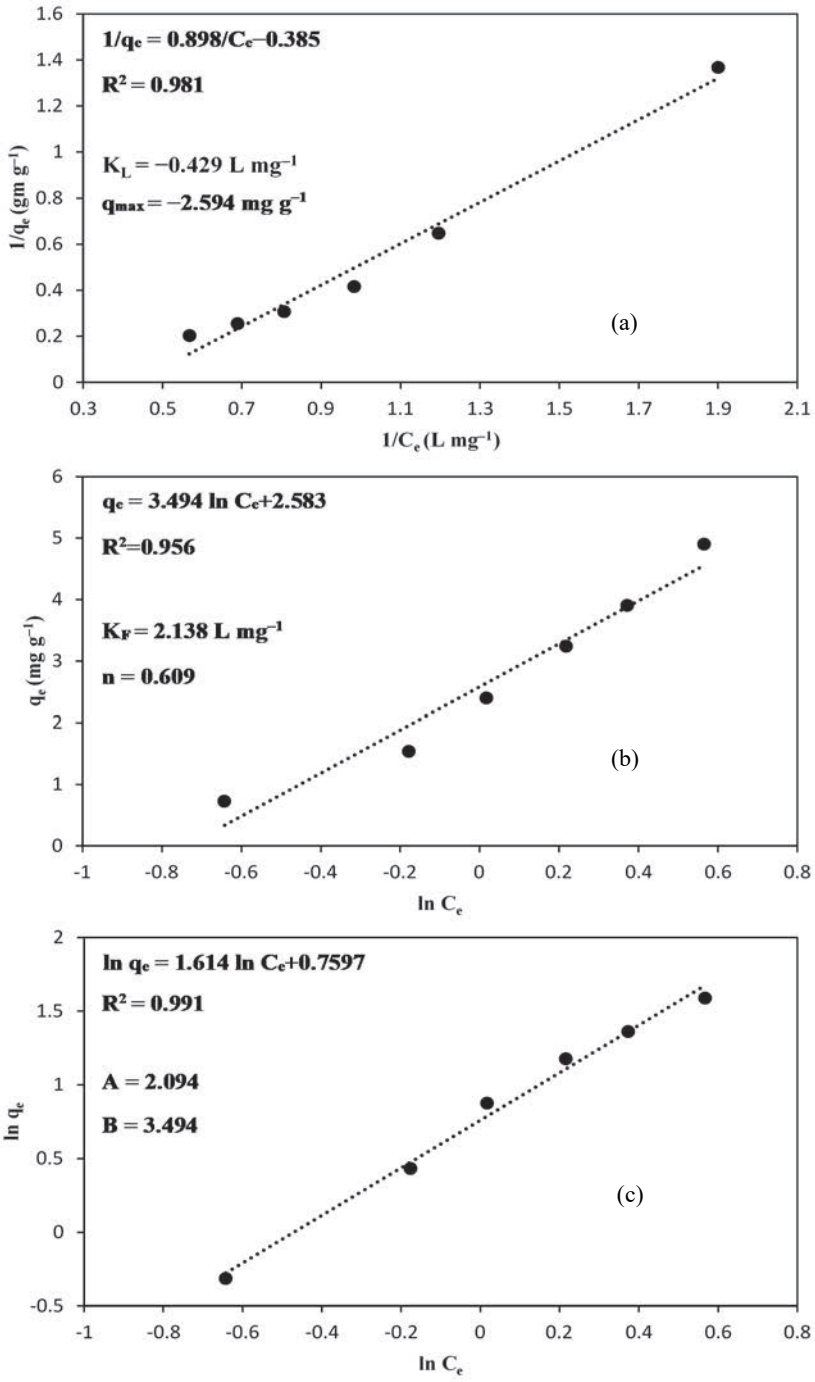

Fig. 9. Langmuir (a), Temkin (b) and Freundlich (c) isotherms for the adsorption of MG onto the Fe_3O_4@SiO_2-ESFO. (Conditions: solution volume: 100 mL; MG concentration: 15.0 mg L^{-1}; sorbent mass: 0.27 g; temprature:30°C; contact time: 15 min; pH: 6.15)

Table 4. The kinetic constants for the adsorption of MG on the Fe_3O_4@SiO_2-ESFO

C_0 (mg L^{-1})	q_e^{exp} (mg g^{-1})	*Pseudo–first order kinetic model*			*Pseudo–second order kinetic model*		
		k_1 (min^{-1})	q_e^{cal} (mg g^{-1})	R^2	k_2 (g mg^{-1} min^{-1})	q_e^{cal} (mg g^{-1})	R^2
15.0	4.97	0.189	0.376	0.939	1.828	5.00	0.999

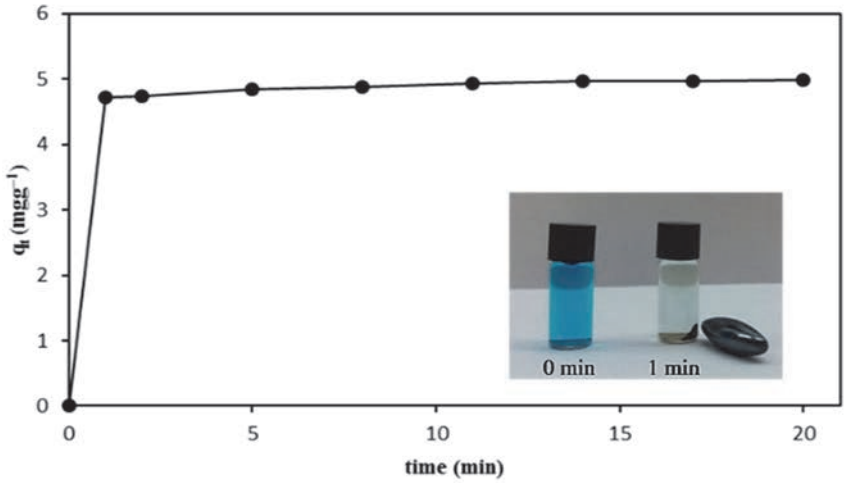

Fig. 10. Effect of contact time on the adsorption capacity of MG onto Fe_3O_4@SiO_2-ESFO. The inset of Figure shows the change in the color of MG solution in the presence of nanocomposite in aqueous solution. (Conditions: solution volume: 100 mL; MG concentration: 15.0 mg L^{-1}; sorbent mass: 0.27 g; Temprature:30°C; pH: 6.15)

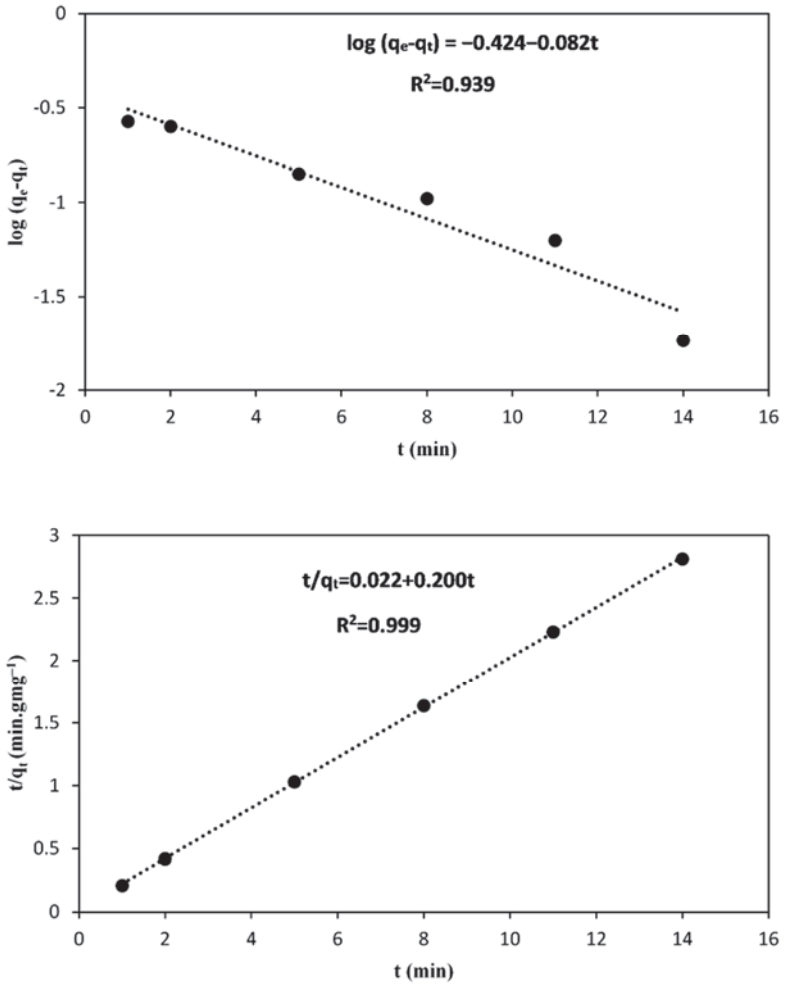

Fig. 11. Pseudo-first-order (a) and pseudo-second-order (b) kinetic models for adsorption of MG onto Fe_3O_4@SiO_2-ESFO. (Conditions: solution volume: 100 mL; MG concentration: 15.0 mg L^{-1}; sorbent mass: 0.27 g; Temprature:30°C; pH: 6.15)

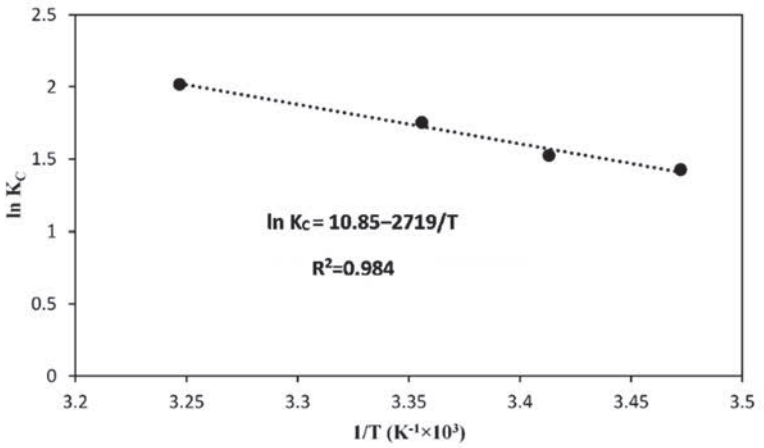

Fig. 12. Plot of ln K_C versus 1/T for the prediction of thermodynamic parameters for the adsorption of MG onto Fe_3O_4@SiO_2-ESFO. (Conditions: solution volume: 100 mL; MG concentration; 15.0 mg L^{-1}; sorbent mass; 0.27 g; contact time: 15 min; pH: 6.15)

Table 5. Thermodynamic parameters for adsorption of MG on the Fe_3O_4@SiO_2-ESFO

T (K)	*ln K_c*	*ΔG^o (kJ mol^{-1})*	*ΔH^o (k mol^{-1})*	*ΔS^o (kJ mol^{-1} K^{-1})*
288	1.43	-3.38	22.61	0.09
293	1.53	-3.83		
298	1.76	-4.28		
308	2.02	-5.18		

Table 6. Comparison with other reported magnetic adsorbents

Adsorbent	*Adsorption capacity (mg g^{-1})*	*Uptake time (min)*	*Removal efficiency (%)*	*Reference*
PANI[a]– $NiFe_2O_4$	4.09	210	95.2	(Patil and Shrivastava, 2015)
Fe_2O_3 -AC[b]	29.32	6.8	85.3	(Saad and Tahir, 2017)
PANI –Fe_3O_4	240	210	95.0	(Mahto et al., 2014)
Alg[c]–Fe_3O_4	47.84	20	82.0	(Mohammadi et al., 2014)
Fe_3O_4@SiO_2-NH_2	173	40	90.0	(Sun et al., 2015)
Fe_3O_4-SiO_2-ESFO	4.97	5.8	90.0	This work

[a]*polyaniline;* [b]*activated carbon;* [c]*sodium alginate*

4. Conclusions

In this work, Fe_3O_4@SiO_2-ESFO was developed as a new nanosorbent for the rapid removal of MG from the aqueous solutions. This sorbent has hydrophobic surface and polar functional moieties, which render it promising for removing MG from the aqueous solution samples.

Due to the presence of hydrophilic polar functional groups, it can be easily dispersed in aqueous solution. Also, because the surface of nanosorbent is hydrophobic, MG can be easily adsorbed by Fe_3O_4@SiO_2-ESFO and the equilibrium condition could be achieved within few minutes.

A Box-Behnken design (BBD) was employed for the determination of optimized experimental conditions for MG removal. The results showed that about 90% of MG can be removed under the optimal experimental conditions including pH value of 6.15, sorbent amount of 0.27 g, temperature of 30°C, and the sonication time of 5.8 min. The isotherm models (Langmuir, Freundlich and Tempkin) were evaluated to depict the mechanism of interaction of the MG with Fe_3O_4@SiO_2-ESFO, and according to the results, the equilibrium data were best described by the Freundlich model. The thermodynamic parameters including ΔG^o, ΔH^o and ΔS^o demonstrated that the MG sorption on Fe_3O_4@SiO_2-ESFO was endothermic and spontaneous phenomena in nature.

Finally, results showed that the kinetic of the adsorption process was best described by pseudo-second order mechanism.

Acknowledgements

The authors are grateful to the PNU Research Council for financial support of this research.

References

Al-Degs Y.S., El-Barghouthi M.I., El-Sheikh A.H., Walker G.M., (2008), Effect of solution pH, ionic strength, and temperature on adsorption behavior of reactive dyes on activated carbon, *Dyes and Pigments*, **77**, 16-23.

Avisar D., Primor O., Gozlan I., Mamane H., (2010), Sorption of sulfonamides and tetracyclines to

montmorillonite clay, *Water, Air and Soil Pollution*, **209**, 439-450.

Aysu T., (2015), Removal of crystal violet and methylene blue from aqueous solutions by activated carbon prepared from *Ferula orientalis*, *International Journal of Environmental Science and Technology*, **12**, 2273-2284.

Bai L., Mei B., Guo Q.Z., Shi Z.G., Feng, Y.Q., (2010), Magnetic solid-phase extraction of hydrophobic analytes in environmental samples by a surface hydrophilic carbon-ferromagnetic nanocomposite, *Journal of Chromatography A*, **1217**, 7331-7336.

Barcena H., Tuachi A., Zhang Y., (2017), Teaching green chemistry with epoxidized soybean oil, *Journal of Chemical Education*, **94**, 1314-1318.

Bharathi K.S., Ramesh S.T., (2013), Removal of dyes using agricultural waste as low-cost adsorbents: a review, *Applied Water Science*, **3**, 773-790.

Bingöl D., Veli S., Zor S., Özdemir U., (2012), Analysis of adsorption of reactive azo dye onto $CuCl_2$ doped polyaniline using Box-Behnken design approach, *Synthetic Metals*, **162**, 1566-1571.

Bouchareb B., Benaniba M.T., (2008), Effects of epoxidized sunflower oil on the mechanical and dynamical analysis of the plasticized poly(vinyl chloride), *Applied Polymer*, **107**, 3442-3450.

Cai Z., Sun Y., Liu W., Pan F., Sun P., Fu J., (2017), An overview of nanomaterials applied for removing dyes from wastewater, *Environmental Science and Pollution Research*, **24**, 15882-15904.

Chen R., Zhang C., Kessler M.R., (2015), Polyols and polyurethanes prepared from epoxidized soybean oil ring-opened by polyhydroxy fatty acids with varying OH numbers, *Journal of Applied Polymer Science*, **132**, 41213 41223.

Collivignarelli M.C., Abbà A., Frattarola A., Miino M.C., Padovani S., Katsoyiannis I., Torretta V., (2019), Legislation for the reuse of biosolids on agricultural land in Europe: Overview, *Sustainability*, **11**, 6015-6037.

Collivignarelli M.C., Abbà A., Miino M.C, Damiani S., (2019), Treatments for color removal from wastewater: State of the art, *Journal of Environmental Management*, **236**, 727-745.

Collivignarelli M.C., Canato M., Abbà A., Miino M.C., (2019), Biosolids: What are the different types of reuse, *Journal of Cleaner Production*, **238**, 1-58.

Delsouz Khaki M.R., Saleh Shafeeyan M., Abdul Raman A.A., Daud W.M.A.W., (2017), Application of doped photocatalysts for organic pollutant degradation - A review, *Journal of Environmental Management*, **198**, 78-94.

Dinda S., Patwardhan A.V., Goud V.V., Pradhan N.C., (2008), Epoxidation of cottonseed oil by aqueous hydrogen peroxide catalysed by liquid inorganic acids, *Bioresource Technology*, **99**, 3737-3744.

El-Sayed G.O., (2011), Removal of methylene blue and crystal violet from aqueous solutions by palm kernel fiber, *Desalination*, **272**, 225-232.

Faraji M., Yamini Y., Rezaee M., (2010), Magnetic nanoparticles: Synthesis, stabilization, functionalization, characterization, and applications, *Journal of the Iranian Chemical Society*, **7**, 1-37.

Fiol N., Villaescusa I., (2009), Determination of sorbent point zero charge: usefulness in sorption studies, *Environmental Chemistry Letters*, **7**, 79-84.

Fonseca B., Maio H., Quintelas C., Teixeira A., Tavares T., (2009), Retention of Cr(VI) and Pb(II) on a loamy sand soil: Kinetics, equilibria and breakthrough, *Chemical Engineering Journal*, **152**, 212-219.

Foo K.Y., Hameed B., (2010), An overview of dye removal via activated carbon adsorption process, *Journal Desalination and Water Treatment*, **19**, 255-274.

Giakisikli G., Anthemidis A.N., (2013), Magnetic materials as sorbents for metal/metalloid preconcentration and/or separation. A review, *Analytica Chimica Acta*, **789**, 1-16.

Grigoraș C., Simion A., Favier L., Gavrilă L., (2020), Congo red removal from aqueous effluents by adsorption on cherry stones activated carbon, *Environmental Engineering and Management Journal,* **19**, 247-254.

Guimarães Gusmão K.A., Alves Gurgel L.V., Sacramento Melo T. M., Gil L.F., (2012), Application of succinylated sugarcane bagasse as adsorbent to remove methylene blue and gentian violet from aqueous solutions - Kinetic and equilibrium studies, *Dyes and Pigments*, **92**, 967-974.

Hameed B.H., Ahmad A.A., Aziz N., (2007), Isotherms, kinetics and thermodynamics of acid dye adsorption on activated palm ash, *Chemical Engineering Journal*, **133**, 195-203.

Hayat H., Mahmood Q., Pervez A., Bhatti Z.A., Baig S.A., (2015), Comparative decolorization of dyes in textile wastewater using biological and chemical treatment, *Separation and Purification Technology*, **154**, 149-153.

Hemmati S., Mehrazin L., Ghorban H., Garakani S.H., Mobaraki T.H., Mohammadi P., Veisi H., (2018), Green synthesis of Pd nanoparticles supported on reduced graphene oxide, using the extract of Rosa canina fruit, and their use as recyclable and heterogeneous nanocatalysts for the degradation of dye pollutants in water, *RSC Advances*, **8**, 21020-21028.

Ho Y.S., Wase D.A.J., Forster C.F., (1996), Kinetic studies of competitive heavy metal adsorption by sphagnum moss peat, *Environmental Technology*, **17**, 71-77.

Huang X., Liu Y., Liu S., Tan X., Ding Y., Zeng G., Zhou Y., Zhang M., Wang S., Zheng B., (2016), Effective removal of Cr(vi) using β-cyclodextrin–chitosan modified biochars with adsorption/reduction bifuctional roles, *RSC Advances*, **6**, 94-104.

Jirankova H., Mrazek J., Dolecek P., Cakl J., (2010), Organic dye removal by combined adsorption-membrane separation process, *Desalination and Water Treatment*, **20**, 96-101.

Jocic S., Miladinovic D., Kaya Y., (2015), *Breeding and Genetics of Sunflower*, In: *Sunflower: Chemistry, Production, Processing, and Utilization*, Martínez Force E., Dunford N.T., Salas J. (Eds.), AOCS Press, Urbana, 1-26.

Kaner D., Saraç A., Şenkal B.F., (2010), Removal of dyes from water using crosslinked aminomethane sulfonic acid based resin, *Environmental Geochemistry and Health*, **32**, 321-325.

Karadag D., Akgul E., Tok S., Erturk F., Kaya M.A., Turan M., (2007), Basic and reactive dye removal using natural and modified zeolites, *Journal of Chemical and Engineering Data*, **52**, 2436-2441.

Kooh M.R., Lim L.B., Lim L.H., Dahri M.K., (2016), Separation of toxic rhodamine B from aqueous solution using an efficient low-cost material, *Azolla pinnata*, by adsorption method, *Environmental Monitoring and Assessment*, **188**, 108-123

Kulshrestha P., Giese R.F., Aga D.S., (2004), Investigating the molecular interactions of oxytetracycline in clay and organic matter: Insights on factors affecting its mobility in soil, *Environmental Science and Technology*, **38**, 4097-4105.

Lee K.W., Hailan C., Yinhua J., Kim Y.W., Chung K.W., (2008), Modification of soybean oil for intermediates by epoxidation, alcoholysis and amidation, *Korean Journal of Chemical Engineering*, **25**, 474-482.

Luo Z.Y., Li Z.Y., Liu H.Y., Tang M.Q., Shi Z.G., (2015), Click chemistry-based synthesis of water-dispersible hydrophobic magnetic nanoparticles for use in solid phase extraction of non-steroidal anti-inflammatory drugs, *Microchimica Acta*, **182**, 2585-2591.

Maiti B., Rathore A., Srivastava S., Shekhawat M., Srivastava P., (2011), Optimization of process parameters for ethanol production from sugar cane molasses by *Zymomonas mobilis* using response surface methodology and genetic algorithm, *Applied Microbiology and Biotechnology*, **90**, 385-395.

Mahto T.K., Chowdhuri A.R., Sahu S.K., (2014), Polyaniline-functionalized magnetic nanoparticles for the removal of toxic dye from wastewater, *Journal of Applied Polymer Science*, **131**, 40840.

Mohammad M., Maitra S., Dutta B.K., (2018), Comparison of activated carbon and physic seed hull for the removal of malachite green dye from aqueous solution, *Water, Air and Soil Pollution*, **229**, 1-14.

Mohammadi A., Daemi H., Barikani M., (2014), Fast removal of malachite green dye using novel superparamagnetic sodium alginate-coated Fe_3O_4 nanoparticles, *International Journal of Biological Macromolecules*, **69**, 447-55.

Narute P., Palanisamy A., (2015), Study of the performance of polyurethane coatings derived from cottonseed oil polyol, *Journal of Coatings Technology and Research*, **13**, 171-179.

Nekoeinia M., Kabiri Dehkordi M., Kolahdoozan M., Yousefinejad S., (2016), Preparation of epoxidized soybean oil-grafted Fe_3O_4–SiO_2 as a water-dispersible hydrophobic nanocomposite for solid-phase extraction of Rhodamine B, *Microchemical Journal*, **129**, 236-242.

Nidheesh P.V., Gandhimathi R., Ramesh S.T., (2013), Degradation of dyes from aqueous solution by Fenton processes: a review, *Environmental Science and Pollution Research*, **20**, 2099-2132.

O'Brien R.D., (2004), *Fats and Oils: Formulating and Processing for Applications*, 2nd Edition, CRC Press, New York, 29-30.

O'Keefe S.F., Pike O.A., (2010), *Fat Characterization*, In: *Food Analysis*, Nielsen S.S. (Eds.), Springer, New York Dordrecht Heidelberg London, 239-260.

Panahi S., Sardarian A.R., Esmaeilzadeh F., Mowla D., (2018), Synthesize and characterization of chitosan and silica supported on Fe_3O_4 nanoparticles for the adsorption and removal of asphaltene molecules from crude oil, *Materials Research Express*, **5**, 095022.

Patil M.R., Shrivastava V.S., (2015), Adsorption of malachite green by polyaniline-nickel ferrite magnetic nanocomposite: an isotherm and kinetic study, *Applied Nanoscience*, **5**, 809-816.

Purbaya M., Nor H.M., Suwardin D., (2015), Synthesis of sunflower oil based elastomer and its characterization by using spectroscopic techniques, *Macromolecular Symposia*, **353**, 161-167.

Rahimi R., Maleki A., Maleki S., Morsali A., Rahimi M.J, (2014), Synthesis and characterization of magnetic dichromate hybrid nanomaterials with triphenylphosphine surface modified iron oxide nanoparticles (Fe_3O_4@SiO_2@PPh_3@$Cr_2O_7^{2-}$), *Solid State Sciences*, **28**, 9-13.

Ruan W., Hu J., Qi J., Hou Y., Zhou C., Wei X., (2019) Removal of dyes from wastewater by nanomaterials: A review, *Advanced Materials Letters*, **10**, 9-20.

Saad M., Tahir H., (2017), Synthesis of carbon loaded γ-Fe_2O_3 nanocomposite and their applicability for the selective removal of binary mixture of dyes by ultrasonic adsorption based on response surface methodology, *Ultrasonics Sonochemistry*, **36**, 393-408.

Sahan T., Ozturk D., (2014), Investigation of Pb(II) adsorption onto pumice samples: application of optimization method based on fractional factorial design and response surface methodology, *Clean Technologies and Environmental Policy*, **16**, 819-831.

Salimon J., Mudhaffar Abdullah B., Yusop R., Salih N., (2014), Synthesis, reactivity and application studies for different biolubricants, *Chemistry Central Journal*, **8**, 16-27.

Sarayu K., Sandhya S., (2012), Current technologies for biological treatment of textile wastewater - A Review, *Applied Biochemistry and Biotechnology*, **167**, 645-661.

Savva I., Marinica O., Papatryfonos C.A., Vekas L., Krasia-Christoforou T., (2015), Evaluation of electrospun polymer–Fe_3O_4 nanocomposite mats in malachite green adsorption, *RSC Advances*, **5**, 16484-16496.

Senthil Kumar P., Ramalingam S., Senthamarai C., Niranjanaa M., Vijayalakshmi P., Sivanesan S., (2010), Adsorption of dye from aqueous solution by cashew nut shell: Studies on equilibrium isotherm, kinetics and thermodynamics of interactions, *Desalination*, **261**, 52-60.

Sun L., Hu S., Sun H., Guo H., Zhu H., Liu M., Sun H., (2015), Malachite green adsorption onto Fe_3O_4@SiO_2-NH_2: isotherms, kinetic and process optimization, *RSC Advances*, **5**, 11837-11844.

Tang M., Wang Q., Jiang M., Xu L., Shi Z.G., Zhang T., Liu Y., (2014), Magnetic solid-phase extraction based on methylcellulose coated-Fe_3O_4–SiO_2–phenyl for HPLC-DAD analysis of sildenafil and its metabolite in biological samples, *Talanta*, **130**, 427-432.

Valipour A., Abbasitabar F., Zare-Shahabadi V., (2020), Zinc hydroxide nanoparticles-modified clay for ultrasound-assisted removal of methylene blue, *Environmental Engineering and Management Journal,* **19**, 453-466.

Veisi H., Razeghi S., Mohammadi P., Hemmati S., (2019), Silver nanoparticles decorated on thiol-modified magnetite nanoparticles (Fe_3O_4/SiO_2-Pr-S-Ag) as a recyclable nanocatalyst for degradation of organic dyes, *Materials Science and Engineering: C*, **97**, 624-631.

Verma A.K., Dash R.R., Bhunia P., (2012), A review on chemical coagulation/flocculation technologies for removal of color from textile wastewaters, *Journal of Environmental Management*, **93**, 154-168.

Vlachos N., Skopelitis Y., Psaroudaki M., Psaroudaki V., Chatzilazarou A., Tegou E., (2006), Applications of Fourier transform-infrared spectroscopy to edible oils, *Analytica Chimica Acta*, **573-574**, 459-465.

Vlček T., Petrović Z.S., (2006), Optimization of the chemoenzymatic epoxidation of soybean oil, *Journal of the American Oil Chemists Society*, **83**, 247-252.

Xiong W., Hu D., (2019), Fabrication of phosphonium bamboo cellulose by triphenylphosphine: preparation, characterization, and adsorption of Acid Black 24, *Environmental Science and Pollution Research*, **26**, 1880-1891.

Yagub M.T., Sen T.K., Afroze S., Ang H.M., (2014), Dye and its removal from aqueous solution by adsorption: A

review, *Advances in Colloid and Interface Science*, **209**, 172-184.

Žalac S., Kallay, N., (1992), Application of mass titration to the point of zero charge determination, *Journal of Colloid and Interface Science*, **149**, 233-240.

Zangeneh H., Zinatizadeh A.A.L., Habibi M., Akia M., Hasnain I.M., (2015), Photocatalytic oxidation of organic dyes and pollutants in wastewater using different modified titanium dioxides: A comparative review, *Journal of Industrial and Engineering Chemistry*, **26**, 1-36.

Zhao S.Y., Lee, D.G., Kim C.W., Cha H.G., Kim Y.H., Kang Y.S., (2006), Synthesis of magnetic nanoparticles of Fe_3O_4 and $CoFe_2O_4$ and their surface modification by surfactant adsorption, *Bulletin Korean Chemical Society*, **27**, 237-241.